# Wetting and Contact-Angle Hysteresis: Density Asymmetry and van der Waals Force

Fei Wang (王飞)●*
*Institute for Applied Materials-Microstructure Modelling and Simulation (IAM-MMS),
Karlsruhe Institute of Technology (KIT), Strasse am Forum 7, 76131 Karlsruhe, Germany
and Institute of Nanotechnology (INT), Karlsruhe Institute of Technology (KIT),
Hermann-von-Helmholtz-Platz 1, 76344 Eggenstein-Leopoldshafen, Germany*

Britta Nestler
*Institute for Applied Materials-Microstructure Modelling and Simulation (IAM-MMS),
Karlsruhe Institute of Technology (KIT), Strasse am Forum 7, 76131 Karlsruhe, Germany;
Institute of Nanotechnology (INT), Karlsruhe Institute of Technology (KIT),
Hermann-von-Helmholtz-Platz 1, 76344 Eggenstein-Leopoldshafen, Germany
and Institute of Digital Materials Science, Karlsruhe University of Applied Sciences, Moltkestrasse 30, 76133 Karlsruhe, Germany*

A droplet depositing on a solid substrate leads to the wetting phenomenon, such as dew on plant leaves. On an ideally smooth substrate, the classic Young's law has been employed to describe the wetting effect. However, no real substrate is ideally smooth at the microscale. Given this fact, we introduce a surface composition concept to scrutinize the wetting mechanism via considering the liquid-gas density asymmetry and the fluid-solid van der Waals interaction. The current concept enables one to comprehend counterintuitive phenomenon of contact-angle hysteresis on a smooth substrate and increase of contact angle with temperature as well as gas bubble wetting.

When a droplet is deposited on a solid substrate, an apparent contact angle $\theta$ (cf. Fig. 1) is formed at the equilibrium state [1]. This phenomenon is broadly observed in daily lives, e.g., dew on leaves, and in industrial applications, such as inkjet printing. On an ideally smooth substrate, the apparent contact angle $\theta$ is unique according to Young's theory [2], known as Young's law. Young's theory has been widely applied to interpret a variety of wetting effect in physics, chemistry, biology, materials, and many other interdisciplinary topics [3–7]. However, in reality, there is no rigorous smooth homogeneous surface, leading to the deviation of the real contact angle from Young's prediction as well as the so-called contact-angle hysteresis [8], corresponding to multiple energy minima of the system [9–11]. The complexities of the contact-angle hysteresis [12] and the related mysterious mechanisms give rise to a big challenge for cognition of the wetting phenomenon and its applications.

To understand the wetting effect on a realistic surface, a number of quintessential theories have been developed [7,13–15]. One well-known theory is the Cassie-Wenzel

theory [16–18], providing a correction to Young's prediction when macroscopic surface roughness affects the effective contact area between the solid and the fluids. In most existing theories, the contact-angle hysteresis is attributed to macroscopic roughness [19–21]. However, it has been observed in experiments that contact-angle hysteresis can occur on a smooth homogeneous substrate [22–24] and even appears on a liquid surface [25], where there is no macroscopic roughness. These experimental
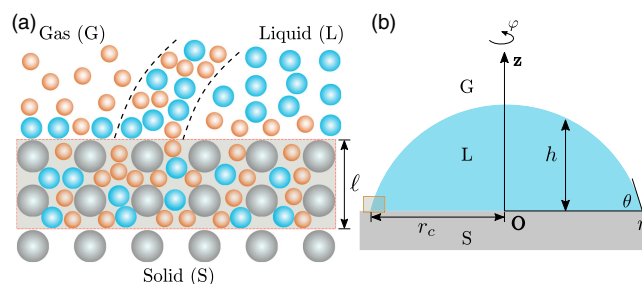


FIG. 1. (a) Sketch for the surface composition concept when a liquid droplet ($L$) is deposited on a solid substrate ($S$) in a gas phase ($G$). The average volume fraction of the liquid species penetrating into solid at the microscale is denoted by $\phi$. Between the dashed lines: $L$-$G$ diffuse interface. Gray, solid; cyan, water; orange, gas. (b) Schematic sectional view in the cylinder coordinate $(r, \varphi, z)$.

observations seem to be counterintuitive and fall out of the scope of Young's and Cassie-Wenzel theory.

In this Letter, we introduce an alternative concept of surface composition to scrutinize the wetting effect. The present concept is based on the question that up to which length scale the surface is not rough. As sketched in Fig. 1, we consider a droplet on top of a solid substrate with an apparent contact angle $\theta$ (see Refs. [26,27] for the terminology, such as apparent, advancing, receding, microscopic, and macroscopic contact angles). The liquid, gas, and solid phases are denoted by $L$, $G$, and $S$, respectively. At the microscale, nothing is really smooth; we propose that the liquid and gas phases partially penetrate into the solid phase. We denote the average volume fraction of the liquid phase penetrating into $S$ as $\phi(\mathbf{x})$, $\forall \mathbf{x} \in S$.

For a given droplet volume $V$, the total interfacial energy consists of the droplet cap $\int_A \sigma dA$ and the substrate $\int_S (\gamma_L - \gamma_G)dS + C$, where $C$ is an arbitrary reference constant depending on the surface area of the substrate. The parameters $\sigma$, $\gamma_L$, and $\gamma_G$ denote the $L$-$G$, $L$-$S$, and $S$-$G$ interfacial tensions, respectively. By defining $\Delta\gamma = \gamma_G - \gamma_L$, we express the system interfacial energy in the cylinder coordinate $(r, \varphi, z)$ as [28]

$$E = \int_0^{2\pi} \int_0^{r_c} r\left[\sigma\sqrt{1 + \left(\frac{dh}{dr}\right)^2} - \Delta\gamma\right] dr d\varphi, \quad (1)$$

where $h(r)$ stands for the distance of the $L$-$G$ interface to the substrate and $r_c$ represents the base radius (Fig. 1). The gravity effect may be added to the system energy in Eq. (1); as demonstrated in Ref. [29], the equilibrium contact angle is not modified for fluids with a uniform density and free-slip triple junction [30]. In contrast to the previous assumption of constant interfacial energies, $\gamma_G, \gamma_L = $ const, we here introduce a wall free energy density function $\gamma(\phi)$ as

$$\gamma = \ell\left[p_L\phi + p_G(1-\phi) + \chi\phi(1-\phi) + \chi_L\phi + \chi_G(1-\phi)\right].$$

The expression of the wall free energy is motivated by the phase-field concept [32–35] based on Cahn's theory [31], wherein the free energy density consists of a bulk term $\gamma(\phi)$ and a gradient energy term $\tau(\nabla\phi)^2$ [36–40]. The first two terms account for the internal energy with $p_L = \rho_L\epsilon_L$ and $p_G = \rho_G\epsilon_G$ following the formulation of van der Waals [41], where $\epsilon_i$ $(i = L, G)$ is the internal energy per unit mass. The third term denotes the short-range van der Waals interaction between liquid and gas, as in the Flory-Huggins model [42–45]. The Flory parameter $\chi$ describes the intermolecular potential. The last two terms depict the van der Waals interaction of $S$-$L$ and $S$-$G$, respectively. The parameter $\ell$ depicts the penetration depth of fluids into the solid [cf. Fig. 1(a)].

The necessary equilibrium condition $\partial_{r_c} E = 0$ engenders the well-known Young's law for the contact angle

$$\sigma\cos\theta = \gamma_G - \gamma_L. \quad (2)$$

Substituting the Young's equation into the energy function of Eq. (1) subject to the volume constraint $V = (\pi/3)$ $(r_c/\sin\theta)^3(2 + \cos\theta)(1 - \cos\theta)^2$, we obtain the total interfacial energy of the system as

$$\frac{E}{\sigma(3V\sqrt{\pi})^{2/3}} = \left(2 + \frac{\gamma_G - \gamma_L}{\sigma}\right)^{1/3}\left(1 - \frac{\gamma_G - \gamma_L}{\sigma}\right)^{2/3}. \quad (3)$$

Noteworthily, the equilibrium contact angle still follows Eq. (2) to account for the Young's contact angle, but $\gamma_L$ and $\gamma_G$ are no longer constants but depend on $\phi$. The equilibrium state is obtained via analyzing the energy landscape $E(\phi_L, \phi_G)$ through the principle of energy minimization

$$\left\{\min E(\phi_L, \phi_G) | 0 \le \phi_L \le 1, 0 \le \phi_G \le 1\right\}.$$

By varying $\phi_L$ and $\phi_G$ in the function domain $\Lambda = \{(\phi_L, \phi_G)|0 \le \phi_L \le 1, 0 \le \phi_G \le 1\}$, we obtain a central finding of this work, the energy landscape $E(\phi_L, \phi_G)$, as shown in Fig. 2. Rewriting the wall free energy function as

$$\frac{\gamma}{\ell\chi} = -\phi^2 + \left[1 - \frac{(p_G - p_L) - (\chi_L - \chi_G)}{\chi}\right]\phi + \frac{p_G + \chi_G}{\chi},$$

we comprehend the energy landscape as a result of three forces: (F1) pressure force, $\Delta p = p_G - p_L$, which is due to the density asymmetry; (F2) van der Waals forces, $\Delta\chi = \chi_L - \chi_G$, which determine the wettability of the system when the densities of the two immiscible fluids are almost the same, namely, hydrophilicity when $\Delta\chi < 0$ and hydrophobicity when $\Delta\chi > 0$; (F3) $L$-$G$ intermolecular force $\chi$, which establishes the $L$-$G$ interface. According to the ratio of these three forces, we divide the wetting effect into three categories, (a), (b), and (c).

*Type (a)*: $\chi < \Delta p - \Delta\chi$.—The inequity indicates that the $L$-$G$ intermolecular force is less than the pressure force minus the van der Waals force, which can be further divided into two subtypes: (a)(i): $\chi < \chi_G - \chi_L$, where the two immiscible fluids have almost the same density. This case is the most considered in the literature for modeling a superhydrophilic surface. An example is the water-oil system. (a)(ii): $\chi < \Delta p - \Delta\chi$, the pressure force due to the density difference competing with the van der Waals force. An example is the water-air system. Figure 2(a)(i) shows an exemplary energy landscape for $(\Delta p - \Delta\chi)/\chi = 2$. The equilibrium contact angle according to Eq. (2) is depicted in Fig. 2(a)(ii). As observed in Fig. 2(a)(i), there is only a local minimum at $\phi_L = 1$ and $\phi_G = 0$ in the energy landscape; the contact angle is zero at
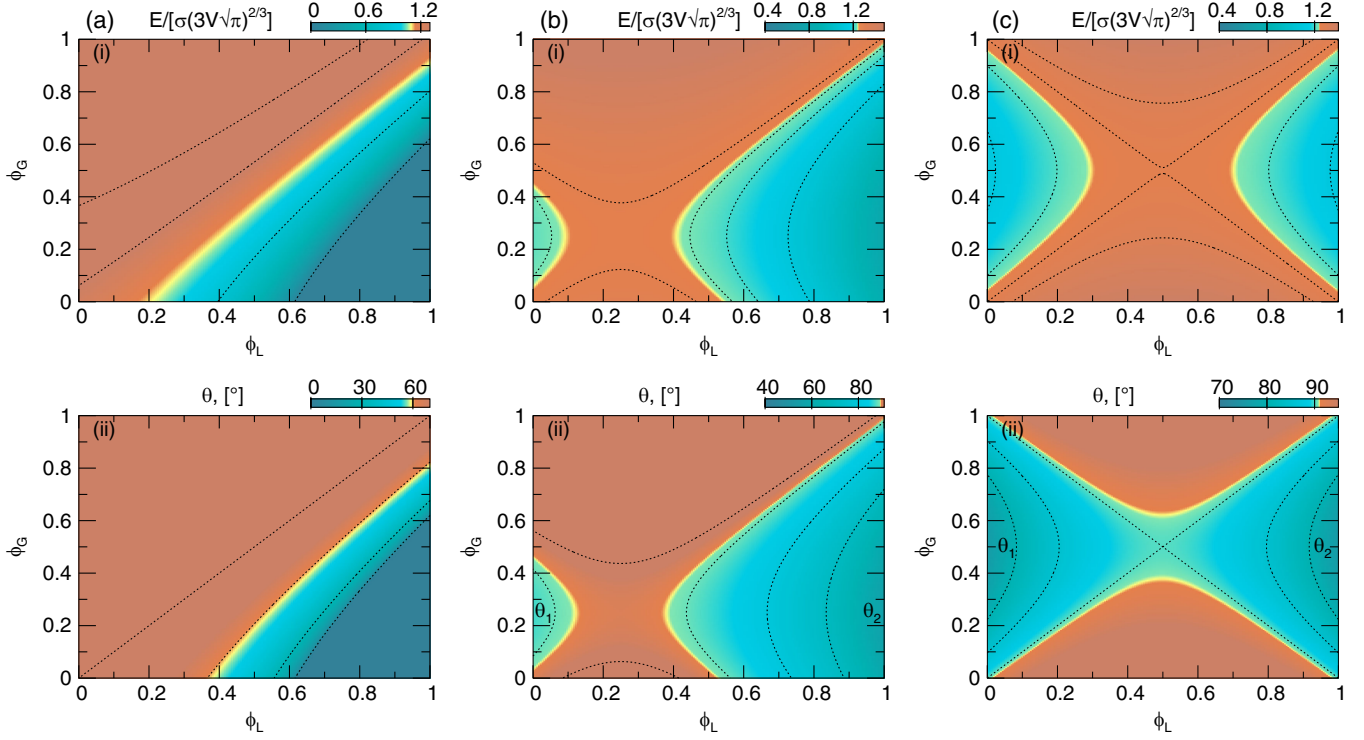
FIG. 2. Energy landscape $E(\phi_L, \phi_G)$ (top) and the map of the Young's contact angle $\theta(\phi_L, \phi_G)$ (bottom) for three types of wetting, classified as (a), (b), and (c). In type (a), there is only a local minimum in the energy landscape (i) and the contact angle at the minimum state is zero (ii). In types (b) and (c), two local minima appear in the energy landscape, resulting in two Young's contact angles $\theta_1$ and $\theta_2$. The parameters in (a), (b), and (c) are $(\Delta p - \Delta \chi)/\chi = 2$, 0.5, and 0, respectively. The contact angle is calculated according to the Young's equation with $\varrho = 1$.

the energy minimum state. Suffice to say, type (a) corresponds to superhydrophilic wetting.

*Type (b)*: $\chi \geq \Delta p - \Delta \chi$.—In contrast to a single energy minimum in type (a), in this case, we observe two local energy minima with distinct contact angles $\theta_1$ and $\theta_2$, as demonstrated in Fig. 2(b) with $(\Delta p - \Delta \chi)/\chi = 0.5$. The difference of these two contact angles leads to a nonzero contact-angle hysteresis (CAH), resulting from the competing effect of density ratio, van der Waals interaction, and intermolecular potential. An increase in the density ratio $\rho_L/\rho_G$ can enhance the CAH. An example for the density variation due to gravity and the change of the contact angle has been recently shown by Tan, An, and Ohl [46]. However, the density distribution is unknown; type (b) wetting can be used to explain some counterintuitive experimental observations of nonzero CAH on a macroscopically smooth substrate [22].

*Type (c)*: $\chi \gg \Delta p - \Delta \chi$, *which is a special case of type (b)*.—By setting $(\Delta p - \Delta \chi)/\chi = 0$, the energy landscape and the corresponding contact angle are shown in Figs. 2(c)(i) and 2(c)(ii), respectively. In this case, the energy landscape becomes symmetric. As in type (b), two local minima also occur in the energy landscape. Differing from type (b), the two contact angles at the energy

minimum state are identical, indicating that there is no CAH, namely, $\Delta \theta = 0°$.

Next, we quantify the contact angle and the CAH as a function of the intermolecular potential $\chi$, the pressure force $\Delta p$, and the van der Waals force $\Delta \chi$. The energy minimum state is obtained via solving the equation system consisting of $\mathcal{E}_1$ and $\mathcal{E}_2$, which is defined as $\mathcal{E}_1$: $\partial E/\partial \phi_G = 0$, $\mathcal{E}_2$: $\partial E/\partial \phi_L = 0$ and leads to the following closed forms for the apparent contact angles:

$$\cos \theta_1 = \varrho \left( 1 - \frac{\Delta p - \Delta \chi}{\chi} \right)^2, \quad (4)$$

$$\cos \theta_2 = \varrho \left( 1 + \frac{\Delta p - \Delta \chi}{\chi} \right)^2, \quad (5)$$

where the scaling factor $\varrho = \ell \chi / 4\sigma$ is a material parameter relating to the penetration depth $\ell$ of the fluid in the solid, the liquid-gas surface tension $\sigma$, and the Flory parameter $\chi$ of liquid-gas. The contact angles $\theta_1$ and $\theta_2$ as a function of the ratio of $(\Delta p - \Delta \chi)/\chi$ are shown in Fig. 3(a) for three exemplary scaling factors, $\varrho = 1$, 0.5, and 0.25 due to the variation of the Gibbs dividing surface [47,48]. We present
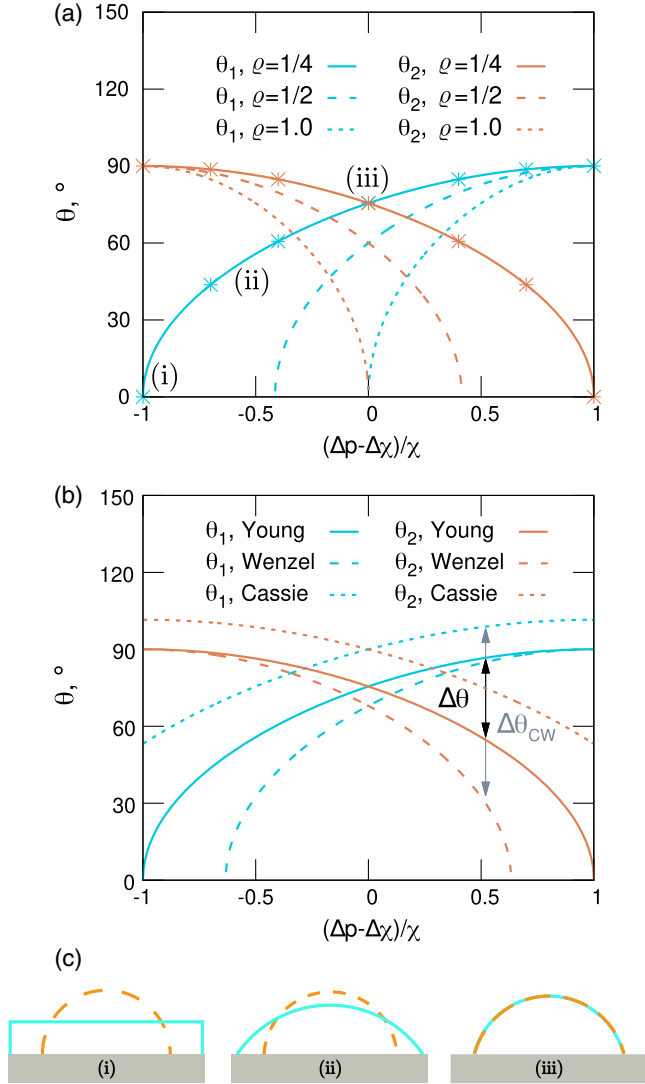
FIG. 3. Contact angle. (a) The contact angle $\theta_1$ (cyan) and $\theta_2$ (orange) as a function of the ratio $(\Delta p - \Delta \chi)/\chi$ for different scaling factors, $\varrho = 1$, 0.5, and 0.25. Stars: numerical simulation of the phase-field model. The labels (i), (ii), and (iii) highlight the setups for the simulation in (c). (b) Comparison with the Cassie-Wenzel theory for $\varrho = 0.25$. The roughness factor $\Upsilon$ in the Wenzel equation and the parameter $\Phi$ in the Cassie equation are set to be 1.2 and 0.8, respectively. (c) Simulation results for $\theta_1$ (cyan) and $\theta_2$ (orange) with $(\Delta p - \Delta \chi)/\chi = -1$ (i), $-0.5$ (ii), and 0 (iii) when $\varrho = 0.25$.

the following remarks and highlights for the results shown in Fig. 3.

(I) *Wettability.*—By varying the ratio $(\Delta p - \Delta \chi)/\chi$ between $-1$ and 1, we obtain all the hydrophobic setup with contact angles between 0° and 90° for both $\theta_1$ and $\theta_2$. The contact angle of 0° and 90° corresponds to the limiting case, $|(\Delta p - \Delta \chi)/\chi| \geq 1$. For $|(\Delta p - \Delta \chi)/\chi| > 1$, the description of the wetting effect via contact angle loses its validity; the wetting state in this case has to be characterized by the energy map presented in Fig. 2.

The hydrophobic setup is realized by replacing $\theta_i$ with $\pi - \theta_i$ ($i = 1, 2$) in Eqs. (4) and (5) and $\theta$ with $\pi - \theta$ in Eq. (2). The energy landscape can be obtained accordingly by replacing $(\gamma_L - \gamma_G)/\sigma$ with $(\gamma_G - \gamma_L)/\sigma$ in Eq. (3).

(II) *Roughness effect.*—For a fixed value of $(\Delta p - \Delta \chi)/\chi$, we always have a nonzero CAH except when $\Delta p = \Delta \chi$ where the two curves of $\theta_1$ and $\theta_2$ intersect. This result can be used to support counterintuitive experimental observation that a nonzero CAH occurs on a smooth substrate [22]. The CAH can be characterized by $\cos \theta_2 - \cos \theta_1 = 4\varrho(\Delta p - \Delta \chi)/\chi$. It should be remarked that the present CAH can be magnified by the macroscopic roughness, as demonstrated in Fig. 3(b). Here, we adopt the Cassie-Wenzel (CW) theory [17,18] to account for the macroscopic roughness via

$$\cos \theta_{i,\text{Wenzel}} = \Upsilon \cos \theta_i, \quad i = 1, 2,$$

$$\cos \theta_{i,\text{Cassie}} = \Phi \cos \theta_i - (1 - \Phi), \quad i = 1, 2,$$

where $\Upsilon$ is the roughness factor and $\Phi$ denotes the contact fraction of solid-liquid beneath the droplet. From the comparative study in Fig. 3(b), we see that, for each contact angle $\theta_i$, the CW theory can lead to CAH (dotted and dashed lines). However, if we compare the Wenzel curve for $\theta_2$ and the Cassie curve for $\theta_1$, we see that the macroroughness enhances the CAH ($\Delta \theta_{\text{CW}}$, gray arrows), but the origin of CAH ($\Delta \theta$, black arrows) is the microroughness. The same conclusion can be drawn when comparing the Cassie curve for $\theta_2$ and Wenzel curve for $\theta_1$.

(III) *Gas bubble wetting.*—From Young's law, $\cos \theta = \gamma_G - \gamma_L$, the contact angle of $\pi - \theta$ is also an energy minimum state, with $\cos(\pi - \theta) = \gamma_L - \gamma_G$, where $\pi - \theta$ is the apparent contact angle of a gas bubble. Apparently, the summation of $\pi - \theta_1$ with $\theta_2$ or $\pi - \theta_2$ with $\theta_1$ is not 180°. This result can be used to comprehend the experimental observation of gas bubble wetting [49,50] and the related CAH [51]. The different wetting behavior of the droplet and gas bubble is attributed to the density asymmetry.

(IV) *Temperature effect.*—The contact angle $\theta_1$ increases with $(\Delta p - \Delta \chi)/\chi$, while $\theta_2$ decreases with $(\Delta p - \Delta \chi)/\chi$. This result can be used to explain experimental observation that the contact angle sometimes increases with temperature [52,53] and sometimes decreases with temperature [54,55]. Assuming that $(\Delta p - \Delta \chi)/\chi$ increases with temperature, we have the decrease of $\theta_2$ with temperature till zero; the other one $\theta_1$ must increase with temperature. The decrease of the contact angle with temperature till zero is consistent with Cahn's wetting transition theory [31] and Adamson's adsorption theory [56]. The increase of the contact angle with temperature is counterintuitive and can be well explained by the present results. Note that advancing and receding contact angles both can increase with

temperature, which correspond to the region $(\Delta p - \Delta \chi)/\chi > 0$ and $(\Delta p - \Delta \chi)/\chi < 0$, respectively.

In addition, we employ phase-field simulation to support the variation of the contact angle with $(\Delta p - \Delta \chi)/\chi$, as shown in Fig. 3(c). The model is well established and validated for various wetting phenomena [28,57]. By fixing the droplet volume and using the interfacial energy at the energy minimal state, we observe the advancing and receding contact angles [Fig. 3(c)(ii)]. The simulation result supports the theoretical calculation quantitatively that there are two distinct contact angles for a fixed droplet volume.

The above derivation assumes that the solid surface is rigorously inert and does not move in space and with time, both microscopically and macroscopically. This treatment is in contrast to a more physically reasonable concept of surface adaptation, as proposed by Butt [58] and Tadmor [59]. When the fluid contacts the solid, the solid reorients, deforms, and swells at the microscale [58,59] and can even protrude to the liquid [60]. By considering surface adaptation, we extend the above derivation into two cases. Case A: static wetting. When the solid is reconstructed microscopically, we consider the change of the solid composition and the modified wall free energy function: $\gamma_s/\ell = \sum_i p_i \phi_i + \sum_{i<j} \chi_{ij} \phi_i \phi_j$, where $\phi_i$ ($i = S, L, G$) stands for the volume concentration of the $i$th component, $p_i$ is the internal energy, and $\chi_{ij}$ characterizes the binary van der Waals interaction. Case A is further divided into two subcategories: (A)(i) The volume fraction of the solid phase is a constant less than but very close to 1. Following the same derivation procedure for Eqs. (4) and (5) with $\sum_{i=G,L} \phi_i = 1$, we obtain the modified contact angles $\theta_1^*$ and $\theta_2^*$ with the correction for the contribution of the van der Waals force: $\Delta \chi^* = \phi_S(\chi_L - \chi_G)$. This result shows reduction consistency with Eqs. (4) and (5) when $\phi_S = 1$ for a rigorously inert solid surface. (A)(ii) The volume fraction of the solid phase is a free parameter, which can lead to macroscopic topological changes [61], like liquid lens, as comprehensively considered in Ref. [47], which is beyond the scope of the current work. (B) Dynamic wetting with contact angle $\vartheta$. For relatively small velocity, the contact angle is assumed to follow Young's law at every time step. By applying Butt's adaptive wetting theory [12,58,62,63] with time relaxation for the interfacial energies, we obtain $\cos \vartheta^a = \cos \theta_1^* - \omega_a e^{-t/\tau_a}$ and $\cos \vartheta^r = \cos \theta_1^* + \omega_r e^{-t/\tau_r}$. A similar formulation can be applied for $\theta_2^*$. Here, $\omega_{a/r}$ and $\tau_{a/r}$ are fitting parameters according to experiments. Note that $\theta_1^*$ and $\theta_2^*$ can be interchanged depending on the advancing and receding properties, in contrast to a unique Young's contact angle in Butt's theory. For relatively large velocity, fluid dynamics has to be taken into account [64–66].

In summary, we have introduced a surface composition concept based on that no substrate is ideally smooth at the microscale. A central finding is the multiple energy minima

in the surface energy landscape and the resulting contact-angle hysteresis. We consider the competing effect of density ratio $\Delta p$, van der Waals interaction $\Delta \chi$, and intermolecule potential $\chi$, leading to a generalized equation of Young's law as

$$\cos \theta_{1,2} = \varrho \left[ 1 \pm (\Delta p - \Delta \chi)/\chi \right]^2. \qquad (6)$$

The scaling factor $\varrho$ is related to the liquid-gas surface tension $\sigma$ and the penetration depth $\ell$ of fluid into the solid at the microscale. This result can be further coupled with Butt's adaptation wetting theory [12,58,62,63]. The present concept can be used to interpret counterintuitive physical phenomenon, such as CAH on a relatively smooth substrate and increase of contact angle with temperature. Moreover, the present work can cope with the knotty wetting phenomenon of a gas bubble.

[*]fei.wang@kit.edu

[1] P.-G. De Gennes, Rev. Mod. Phys. **57**, 827 (1985).
[2] T. Young, Phil. Trans. R. Soc. London **95**, 65 (1805).
[3] H. Lambley, G. Graeber, R. Vogt, L. C. Gaugler, E. Baumann, T. M. Schutzius, and D. Poulikakos, Nat. Phys. **19**, 649 (2023).
[4] Z. Cheng, D. Zhang, X. Luo, H. Lai, Y. Liu, and L. Jiang, Adv. Mater. **33**, 2001718 (2021).
[5] M. Li, C. Li, B. R. Blackman, and S. Eduardo, Int. Mater. Rev. **67**, 658 (2022).
[6] S. Herminghaus, M. Brinkmann, and R. Seemann, Annu. Rev. Mater. Res. **38**, 101 (2008).
[7] F. Wang, Y. Wu, and B. Nestler, Adv. Mater. **35**, 2210745 (2023).
[8] E. Y. Bormashenko, *Wetting of Real Surfaces* (de Gruyter, Berlin, 2018), Vol. 19.
[9] A. Marmur, Adv. Colloid Interface Sci. **50**, 121 (1994).
[10] S. Brandon and A. Marmur, J. Colloid Interface Sci. **183**, 351 (1996).
[11] A. Marmur, Colloids Interfaces **6**, 39 (2022).
[12] H.-J. Butt, J. Liu, K. Koynov, B. Straub, C. Hinduja, I. Roismann, R. Berger, X. Li, D. Vollmer, W. Steffen *et al.*, Curr. Opin. Colloid Interface Sci. **59**, 101574 (2022).
[13] R. Tadmor, Langmuir **37**, 6357 (2021).
[14] L. Makkonen, J. Chem. Phys. **147**, 064703 (2017).
[15] C. Semprebon, G. McHale, and H. Kusumaatmaja, Soft Matter **13**, 101 (2017).
[16] E. Bormashenko, Adv. Colloid Interface Sci. **222**, 92 (2015).
[17] R. N. Wenzel, Ind. Eng. Chem. **28**, 988 (1936).
[18] A. Cassie and S. Baxter, Trans. Faraday Soc. **40**, 546 (1944).
[19] D. Quéré, Annu. Rev. Mater. Res. **38**, 71 (2008).

[20] H. B. Eral, D. 't Mannetje, and J. M. Oh, Colloid Polym. Sci. **291,** 247 (2013).

[21] C. Yang, U. Tartaglino, and B. N. J. Persson, Phys. Rev. Lett. **97,** 116103 (2006).

[22] P. Rahimi and C. Ward, Microgravity Sci. Technol. **16,** 231 (2005).

[23] V. Starov, Colloid Polym. Sci. **291,** 261 (2013).

[24] C. A. Ward and J. Wu, Phys. Rev. Lett. **100,** 256103 (2008).

[25] H. Barrio-Zhang, E. Ruiz-Gutierrez, S. Armstrong, G. McHale, G. G. Wells, and R. Ledesma-Aguilar, Langmuir **36,** 15094 (2020).

[26] A. Marmur, C. Della Volpe, S. Siboni, A. Amirfazli, and J. W. Drelich, Surf. Innov. **5,** 3 (2017).

[27] E. Ruckenstein and G. Berim, *Wetting: Theory and Experiments, Two-Volume Set* (CRC Press, Boca Raton, 2019).

[28] Y. Wu, F. Wang, M. Selzer, and B. Nestler, Phys. Rev. E **100,** 041102(R) (2019).

[29] E. Bormashenko, J. Adhes. Sci. Technol. **34,** 219 (2020).

[30] The variational approach leads to the independence of the equilibrium contact angle (see Ref. [29]) on the gravitational effect, when the density of the fluid is assumed to be uniform thoroughly and the contact line slips freely. The unknown question is whether the density is really uniform throughout the liquid, especially near the solid surface. According to the concept of de Gennes (Ref. [1]) and Cahn (Ref. [31]), the density of the liquid on the solid substrate differs from the bulk of the liquid, known as Cahn's wetting theory. This indicates that there is a spatial variation of the liquid density, especially near the solid surface. The change of the density and the associated energy can change the energy minimization and the equilibrium contact angle.

[31] J. W. Cahn, J. Chem. Phys. **66,** 3667 (1977).

[32] J. Van der Waals, Verhandel/Konink, Akad. Weten **1, 56** (1893).

[33] D. Jacqmin, J. Comput. Phys. **155,** 96 (1999).

[34] P. Yue, J. Fluid Mech. **899,** A15 (2020).

[35] F. Wang, A. Choudhury, C. Strassacker, and B. Nestler, J. Chem. Phys. **137,** 034702 (2012).

[36] The line tension effect may be captured by adding a term $\tau(\nabla\phi)^2$ to the wall free energy function [37,38]. Here, $\tau$ is the gradient energy coefficient. By using the variational calculus $\delta\gamma/\delta\phi = 0$, the term $\tau(\nabla\phi)^2$ is converted into $\tau/r_c$ using the divergence theorem; the sign of $\tau$ is responsible for the positive and negative line tensions. Because of the scattering of the experimental data in the literature [39,40], we omit a further discussion here to avoid potential confusion.

[37] H. Zhang, F. Wang, and B. Nestler, Phys. Rev. E **108,** 054121 (2023).

[38] J. W. Cahn and J. E. Hilliard, J. Chem. Phys. **28,** 258 (1958).

[39] A. Amirfazli and A. Neumann, Adv. Colloid Interface Sci. **110,** 121 (2004).

[40] B. M. Law, S. P. McBride, J. Y. Wang, H. S. Wi, G. Paneru, S. Betelu, B. Ushijima, Y. Takata, B. Flanders, F. Bresme *et al.,* Prog. Surf. Sci. **92,** 1 (2017).

[41] J. S. Rowlinson, J. Stat. Phys. **20,** 197 (1979).

[42] W. Zhang, E. D. Gomez, and S. T. Milner, Phys. Rev. Lett. **119,** 017801 (2017).

[43] F. Wang, P. Altschuh, L. Ratke, H. Zhang, M. Selzer, and B. Nestler, Adv. Mater. **31,** 1806733 (2019).

[44] P. J. Flory, J. Chem. Phys. **10,** 51 (1942).

[45] M. L. Huggins, J. Chem. Phys. **9,** 440 (1941).

[46] B. H. Tan, H. An, and C.-D. Ohl, Phys. Rev. Lett. **130,** 064003 (2023).

[47] L. Schimmele, M. Napiórkowski, and S. Dietrich, J. Chem. Phys. **127,** 164715 (2007).

[48] The length parameter $\ell$ is affected by the choice of the Gibbs dividing surface, which varies from material to material and is generally unknown.

[49] H. A. Stone, J. Fluid Mech. **645,** 1 (2010).

[50] D. Lohse and X. Zhang, Rev. Mod. Phys. **87,** 981 (2015).

[51] J. Drelich, J. Adhes. **63,** 31 (1997).

[52] J. W. Song and L. W. Fan, Adv. Colloid Interface Sci. **288,** 102339 (2021).

[53] M. E. Tadros, P. Hu, and A. W. Adamson, J. Colloid Interface Sci. **49,** 184 (1974).

[54] M. E. Diaz, M. D. Savage, and R. L. Cerro, J. Colloid Interface Sci. **503,** 159 (2017).

[55] F. Wang and B. Nestler, J. Chem. Phys. **154,** 094704 (2021).

[56] A. W. Adamson, J. Colloid Interface Sci. **44,** 273 (1973).

[57] Y. Wu, M. Kuzina, F. Wang, M. Reischl, M. Selzer, B. Nestler, and P. A. Levkin, J. Colloid Interface Sci. **606,** 1077 (2022).

[58] H.-J. Butt, R. Berger, W. Steffen, D. Vollmer, and S. A. Weber, Langmuir **34,** 11292 (2018).

[59] R. Tadmor, P. Bahadur, A. Leh, H. E. N'guessan, R. Jaini, and L. Dang, Phys. Rev. Lett. **103,** 266101 (2009).

[60] A. Leh, H. E. N'guessan, J. Fan, P. Bahadur, R. Tadmor, and Y. Zhao, Langmuir **28,** 5795 (2012).

[61] F. Wang, A. Reiter, M. Kellner, J. Brillo, M. Selzer, and B. Nestler, Acta Mater. **146,** 106 (2018).

[62] W. S. Wong, L. Hauer, A. Naga, A. Kaltbeitzel, P. Baumli, R. Berger, M. D 'Acunzi, D. Vollmer, and H.-J. Butt, Langmuir **36,** 7236 (2020).

[63] X. Li, K. Auepattana-Aumrung, H.-J. Butt, D. Crespy, and R. Berger, J. Chem. Phys. **158,** 144901 (2023).

[64] F. Wang, H. Zhang, Y. Wu, and B. Nestler, J. Fluid Mech. **970,** A17 (2023).

[65] R. Cox, J. Fluid Mech. **168,** 169 (1986).

[66] P. Yue and J. J. Feng, Phys. Fluids **23,** 012106 (2011).